THE MECHANICS OF A SILT-SIZED GOLD TAILING

W. LI[1], M. R. COOP[2], K. SENETAKIS[3*] and F. SCHNAID[4]

Author lists:

W. LI[1], Department of Civil Engineering, The University of Hong Kong, Pokfulam road, Hong Kong. liwei890508@126.com

M. R. COOP[2], Department of Civil, Environmental and Geomatic Engineering, University College London, Chadwick Building, Gower Street, London, UK. m.coop@ucl.ac.uk

K. SENETAKIS[3*], Department of Architecture and Civil Engineering, City University of Hong Kong, Tat Chee Avenue, Kowloon Hong Kong. *Corresponding author: ksenetak@cityu.edu.hk

F. SCHNAID[4], Department of Civil Engineering, Federal University of Rio Grande do Sul, Brazil. fschnaid@gmail.com

Abstract

Tailing dam failures result in irreversible environmental impacts and cause fatalities. In recent years the mechanical behaviour of tailing geo-materials has received more attention by the geomechanics and engineering geology communities in an attempt to understand better their behaviour in the light of designing safer tailing dams. In this study, the mechanical behaviour of a gold tailing from Brazil is thoroughly investigated by conducting a series of compression and shearing tests as well as dynamic element tests. Fabric effects from the sample preparation method, the susceptibility to liquefaction and the possibility of any transitional behaviour are presented and discussed within a soil mechanics framework. Comparisons are made between the present gold tailing and previously published data on other tailings, giving a general view of the mechanics of tailings and the effects of grading. The results show that for this tailing the rate of convergence for different initial densities to the normal compression line is slow, and so the depositional density would affect the volume to far higher stresses than the material would be expected to experience in-situ. For this tailing any fabric effects from the sample preparation method were found to be very small to negligible with respect to small-strain behaviour and critical state behaviour. For different tailings, even if the particle sizes may cover a wide range, the susceptibility to static liquefaction, as determined by the location of the horizontal asymptote of the critical state line in the specific volume-log stress plane, shows no consistent variation. So it can be concluded that neither the pond nor the upper beach tailings are more susceptible.

Keywords: tailings; compression behaviour; shearing behaviour; particle characteristics; geotechnical testing.

1. Introduction

Tailings are the by-products after the mining processes to extract the valuable fractions from ores. The mineralogies, gradings and particle morphologies of tailings vary a lot due to the different composition of the parent ores as well as the different extraction processes they undergo. The most common method to dispose of the tailings is impounding a slurried material within a tailings dam, usually being built with the coarser disposal products. Due to the relatively small particle size and high water content, tailings materials often have a high risk of failure due to liquefaction, caused by either static or seismic loading. Even when the tailings liquefaction is not directly responsible for the initial failure, it can exacerbate a failure because its loss of strength causes it to apply a large hydrostatic force to the dam (e.g. Gens and Alonso 2006). If the dam fails catastrophically the runout of the tailings can be fast and fatal (e.g. Chandler and Tosatti, 1995). Between 1912 and 2014 there were more than 240 tailings dam incidents (WISE 2014). The stability performance has therefore concerned many researchers studying the mechanics of tailings/tailing dams (Okusa and Anma, 1980; Fourie et al., 2001; Zandarin et al., 2009; Carrera et al., 2011; Chang et al., 2011; Bedin et al., 2012; Ozer and Bromwell, 2012; Schnaid et al., 2013; Coop, 2015; Zhang et al., 2015).

In this work, detailed laboratory tests were designed to investigate the mechanical behaviour of a silt-sized gold tailing. Comparisons are then made between the present results and reported data in the literature on different tailings to obtain a general view of their behaviour, covering a broader range of mineralogies, particle characteristics and types of tailing materials. The analysis/comparisons are made within a soil mechanics framework. Emphasis is given to the compression and shearing behaviour, static liquefaction, the possible occurrence of transitional behaviour (as defined by e.g. Martins et al., 2001; Altuhafi and Coop, 2011; Xu and Coop, 2016), sample preparation effects as well as their small-strain stiffness/stiffness anisotropy.

2. Materials and procedures

A silt-sized (gold) tailing material, collected from the Fazenda Brasileira disposal plant in Northeast Brazil, was tested in the study in its "natural" or in-situ grading. The grading curve of the soil is given in Figure 1. The tailing has a fractal grading with fractal dimension D_F of 2.19, obtained using the method proposed by Tyler and Wheatcraft (1992). Fractal gradings can represent a broad range of geological materials often found in nature in terms of grain size distribution (Vallejo, 1996; Hyslip and Vallejo, 1997), and have been reported to have complex behaviour (e.g. Altuhafi and Coop, 2011). In the same figure, the tailing tested by Bedin et al. (2012) and Schnaid et al. (2013) is also given for comparison. The latter comes from the same tailing impoundment but is coarser, which resulted in noticeable particle breakage from the shearing tests reported by Bedin et al. (2012).

The parent ore vein is located within the Rio Itapicurú Greenstone Belt (RIGB). Gold, which is present in a very small percentage, is the benefited ore in the vein, with gangue minerals predominately of quartz, albite, chlorite and sulphides. Ore-dressing, such as crushing and grinding, is done first to expose the beneficial minerals for metallurgical extraction, in which the gold is extracted chemically through a heap leaching system. Several methods for hydraulically placing gold tailings are used: the cyclone system, the spigot system, and even (occasionally) open-end discharge behind the containment wall. The sequence of placement changes continuously using one or other of the downstream, centreline or upstream placement techniques. X-ray diffraction (XRD_D8 Advance) analysis (see Figure 2), was conducted at the Institute of Rock and Soil Mechanics, Chinese Academy of Sciences. The voltage and current used are 40 kV and 40 mA respectively, and the angular range is between 3° and 70°. The Reference Intensity Ratio (RIR) method was used to determine the mineral composition percentages, which indicates that the major minerals within the tailing are quartz (22.1%), albite (25.0%), chlorite (47.1%), and calcite (5.9%). The present finer gold tailing contains twice the quantity of chlorite (which belongs to clay-sized minerals) as the coarser one tested by Bedin et al. (2012), but it did not give any plasticity to the soil. Table 1 gives a summary of basic grading characteristics of the present tailing as well as a number of tailings from previous works which were re-analysed and compared with the results of the present study to obtain a general view of the mechanical behaviour of tailings.

A series of oedometer and triaxial tests was conducted on the gold tailing (summarized in Tables 2 and 3) using front loading oedometer frames. The diameters of the rings used were 50 mm and 30 mm, the latter having a floating ring design in order to reduce wall friction (Rocchi and Coop, 2015; Okewale and Coop, 2017), giving resultant maximum vertical stresses of 7 MPa and 20 MPa, respectively. This helped to investigate better the compression behaviour of the soil at greater pressures. The initial specific volumes are the mean values calculated from the measurements of initial weights, dimensions and water contents (for saturated samples) as well as final ones, accounting for the volume changes during the tests (similar to the calculation procedure described by Rocchi and Coop, 2014). For the triaxial tests, most of the samples were tested in a conventional apparatus, with maximum working cell pressure of 700 kPa. A high pressure triaxial with a maximum cell pressure of 7 MPa was also used for a limited number of tests to examine the behaviour over a broader range of pressures. For both apparatus, the sample size was 38 mm in diameter and 76 mm in height. The samples were first saturated with initial flushing using CO_2 to accelerate the process and then they were isotropically compressed and sheared under conventional drained (CID) or undrained (CIU) conditions. Reconstituted samples were used since intact ones were not possible to obtain from this tailing structure. Three different sample preparation methods were adopted to identify any effects of fabric: dry compaction, wet compaction and slurry (details are given in Tables 2 and 3). Even though the intention was to reproduce in-situ states, the construction of samples with different preparation methods gives some more general insights.

A number of samples was also prepared and tested with bender elements inserted in a Bishop and Wesley (1975) apparatus. Details of the samples are given in Table 4. The bender elements were configured in three different directions, allowing the investigation of elastic stiffness and stiffness anisotropy (details in Li and Senetakis, 2017). The three components of shear stiffness could be measured; G_{vh}, G_{hv} and G_{hh}. In each case a single shot sine wave was used, interpreted using the first arrival method and checking a range of input frequencies to ensure that the arrival time was not a function of frequency. All the samples were prepared in a split mould of 50 mm internal diameter and 100 mm in length using two different methods: dry compaction and slurry. By preparing samples with these two different methods, apart from achieving different initial void ratios, the effects of the preparation method on the elastic stiffness, G_{max}, and any possible anisotropy were investigated.

3. Results and discussion

3.1 Compression behaviour

Based on the oedometer test results in Figure 3, it can be seen that the compression curves from different initial densities give a relatively slow convergence and a unique NCL cannot be obtained even when the vertical stresses reach 7 MPa. The accuracies of the initial specific volumes are about ±0.02, estimated from the differences between values calculated by different means (see Rocchi and Coop, 2014), which is much lower than the difference (0.1) between the specific volumes of the loosest and densest samples at 7 MPa, so the non-convergence is significant. In contrast, in the two floating ring oedometer tests (No.9 and No.10), in which the maximum vertical stresses reached 20 MPa, the compression curves are finally just about convergent to a unique one dimensional normal compression line (1D-NCL), which means that the convergence of the curves takes place at very high pressures that the tailing will not experience in-situ. Based on Ponzoni et al. (2014), the m value was quantified from the v_{final}-

$v_{initial}$ graph, which is the slope of the line defined by all the v_{final}-$v_{initial}$ points. In this study the specific volumes were taken at 7MPa and 20kPa, respectively (Figure 4). Error bars based on the estimated accuracy of the specific volumes for each test are shown, indicating that the m value at 7 MPa of 0.13 is significant. At 20 MPa vertical stress, the compression curves nearly converge and so the m value would be close to 0, which means that differences of initial specific volume that result from the initial fabric can be erased by large strains at very high pressures. While the soil is not strictly transitional in that convergence can be brought about within the strains and stresses available, it is at least "slowly convergent". Stresses in a typical tailings lagoon are much less than applied here and so the depositional density would affect the in-situ specific volume. From Figure 4, it can also be seen that, despite some scatter, the data points from different sample preparation methods define a unique line, which means that the initial fabrics that might arise from different sample preparation methods do not affect the convergence.

3.2 Shearing behaviour

3.2.1 Stress-strain data

The stress-strain behaviour of the gold tailing under drained and undrained conditions is shown in Figure 5. The stress-strain curves at lower confining pressures are expanded in Figure 5(a). For the undrained tests, most of the curves have a similar shape. The initial peak deviatoric stresses typically occur at about 1%-3% axial strain, and then a quasi-steady state is reached, which only lasts for a short interval of strain, after which the shear stress increases again. Most of the undrained tests were sheared to 35%-40% axial strain to reach the critical state. However, in some of the tests, a constant deviatoric stress was still not achieved. In Figure 5(b), the changes of pore water pressure, Δu are normalised by p_0', the mean effective stress at the start of shearing, to allow for the effect of different confining pressures. At the start of shearing, the samples are contractive with positive changes of pore water pressure. With the increase of axial strain, a dilative trend occurs and the pore water pressures begin to decrease, causing the increase of deviatoric stress. As for the deviatoric stresses, it can be seen that not all of the pore water pressures reach constant states, which means that these tests have not quite reached critical states, even at these very large strains. For the drained tests, almost all of the curves show post peak strain-softening after peak states at about 10%-20% axial strain. As shown in Figure 5(c), the volumetric strains are contractive initially and then stabilize quickly for looser samples, while for denser samples they become dilative just before the peak shear stresses are reached. The volumetric strains are all reasonably stable at the end of the tests which means the samples have reached or nearly reached critical states.

3.2.2 Stress paths and critical states

The stress paths are shown in Figure 6, the tests at lower confining pressures (<200 kPa) being expanded again (Figure 6b). Since the end points of the undrained tests are easy to identify, only those for the drained tests are indicated. It can be seen that the end points all define a unique CSL in the q: p' plane and a gradient M of 1.41, so that the critical state angle of shearing resistance, φ'_{cs}, is 34.8^{o}, which is the angle of shearing resistance at large strains (the critical state) and is principally controlled by grading, particle shape and the inter-particle sliding friction. The stress paths of the undrained tests are S-shaped, being contractive until a minimum mean effective stress or phase transformation is reached, with the pore water pressures increasing quickly, and then the behaviour changes to dilative.

The shearing paths together with the 1D-NCL of the gold tailing are shown in Figure 7. Also shown is an isotropic NCL, the location of which is estimated from the isotropic compression paths, the CSL and the 1D-NCL, since none of the isotropic compression stages was to sufficiently high pressure to identify it unambiguously. The end points of the shearing tests, which are highlighted, define a unique CSL, despite some scatter, which means that residual differences in specific volume after the compression, as a result of the slowly convergent behaviour, can be erased by shearing. The slight incompleteness of a few tests, despite the large strains reached, probably adds a little to this scatter, and for the most incomplete test an arrow indicates the direction of travel.

The CSL is curved, and at lower stress levels it is relatively flat while at higher stress levels it tends to be parallel to the 1D-NCL. This curved critical state line gives rise to a changing susceptibility to liquefaction as the stress level increases, similarly to Carrera et al. (2011). The two loosest samples sheared from $p_0' = 20$ kPa nearly reach full static liquefaction, as can be seen from their very low final values of p', but the shearing paths show a small inversion at the end of the tests, probably due to the lateral restraining effect of the membrane at high levels of strain. The very low final p' values arise because the end states lie on the almost horizontal part of the CSL. However, at higher stresses even samples with positive state parameters reach stable critical states at finite and large values of p' since their end states lie on the straight part of the CSL, limiting the p' or volume reduction in shear. Since the initial states of most of the samples lie on the dry side of the critical state line, strong strain softening was not generally observed.

The particle size distributions of the gold tailing samples before and after shearing at 6 MPa are shown in Figure 1. No particle breakage was observed which proves that particle breakage is not a necessary feature of a curved CSL, as also found by Carrera et al. (2011) and in contrast to what was found for the coarser tailing from this site by Bedin et al. (2012), which underwent substantial breakage (Figure 1).

Normalised shearing stress paths are illustrated in Figure 8, where q and p' are divided by the equivalent pressure on the critical state lines, $p_{cs}' = \exp((\Gamma - v)/\lambda)$. The q axis is further normalised by M so that the CSL plots at (1,1). Only the straight part of the CSL at higher stress level is adopted for this normalisation, since it cannot work for the curved part, which would give a very large apparent State boundary surface (SBS) as the p_{cs}' value for a nearly liquefied sample is close to 0. The SBS defines the boundaries above which no stress/volume state can exist (Roscoe et al., 1958; Roscoe and Burland, 1968), The wet side of SBS can be identified from the sample isotropically consolidated to 6 MPa, which is considered to have reached the isotropic NCL. The stress ratio between the isotropic NCL and CSL is about 2.2, which is similar to that of many clays, but the gold tailing is non-plastic and there is a peak in the SBS on the wet side of the CSL, which is a feature of sands (Coop and Lee 1993). It can also be seen that the normalised stress paths for drained and undrained tests have different shapes with the undrained paths showing much more obvious dilative tails, which is another feature of sands.

3.2.3 Effect of preparation method

From the bender element tests (Figure 9), it was revealed that for the two preparation methods, the samples had very similar values of the three different moduli, i.e. $G_{vh} \approx G_{hv} \approx G_{hh}$, which indicates an isotropic fabric. It should be noted that G_{vh} is in some cases not perfectly equal to G_{hv}, as it should be (e.g. Jovicic and Coop 1998; Li and Senetakis, 2017), but the maximum difference is only about 10%. The difference might be attributed to the different boundary conditions between the vertical and lateral bender elements.

In Figure 10, the plots of G_{vh} against p' are shown, comparing the slurry method (S) and compaction method (C). For the compacted, both dry and saturated (sat) samples were tested. The values of shear modulus are normalized with respect to a void ratio function, $f(e)=e^{-0.29}$ (Payan et al. 2016) to eliminate possible effects of initial density. Within the scatter of the data, Figure 10 demonstrates that the method of sample preparation and also saturation did not have any significant effect on the stiffness after its normalization.

Figure 11(a) shows that the stress paths of samples prepared by different methods exhibit similar phase transfer states and dilative tails, the exact shapes being controlled by the initial densities and also the stresses the samples were sheared from, so that the wet compacted sample at 50 kPa has a slightly sharper phase transformation than the slurry sample because it was slightly looser. It was not possible to obtain exactly the same specific volumes with different preparation methods. Figure 11(b) shows that the critical state points from different preparation methods define the same CSL. In summary, any fabric effects arising from the sample preparation method are negligible at small-strains and in terms of critical state behaviour, and any differences of stress path may be explained by the different initial densities of the samples. The behaviour at peak is also affected by the density, and so by the preparation method.

Scanning Electron Microscope (SEM) images were taken, using an Environmental SEM (FEI / Philips XL30 ESEM-FEG), to investigate the fabric of slurry and wet compacted samples (Figure 12). No obvious particle orientation or aggregation can be observed in either samples, which means that the preparation method has little effect on the fabric, as also found by Chang et al (2011) for their gold tailing from the pond. Similar observations were made for other tailings tested by Li (2017) and unpublished data by the authors, using different experimental techniques to obtain samples for SEM images.

3.3. Comparisons between different tailings

3.3.1 Results of this study compared with Bedin et al. (2012)

The results presented in this study are now compared with the study of Bedin et al. (2012), since the two tailings were obtained from the same tailings pond and have similar mineralogies but different gradings. The coarser tailing of Bedin et al. (2012) was also subject to particle breakage while that tested here was not (see Figure 1). Figure 13(a) shows a comparison of the one-dimensional compression behaviour. It can be seen that the coarser sandy tailing has much looser initial densities and the 1D-NCL is much easier to reach, as all the compression curves converge at about 400 kPa vertical stress. For the finer silty tailing, a unique 1D-NCL still cannot be identified even at 7 MPa vertical stress, and the location of the line is only finally determined when the vertical stresses reached 20 MPa. The gradient of the 1D-NCL of the silty tailing is slightly smaller, but what is remarkable is that the normal compression lines are in very similar locations, despite breakage playing an important role in the mechanics of the coarse material but not the finer.

Figure 13(b) shows a comparison of the critical states. The CSLs for the silty and sandy tailings were found to be almost identical at larger stress levels but the horizontal asymptote of the CSL for the silty tailing is above that for the sandy one. The combination of the denser initial states and the higher asymptote would make this silty tailing much less susceptible to static liquefaction, which is the contrary to the few existing studies on the liquefaction of tailings (e.g. Carrera et al. 2011), but does agree with a study on iron tailings by Li (2017). The steepening of the CSL of Bedin et al. (2012) indicates the beginning of particle breakage, while no significant particle breakage was found in this study and yet the CSL is still curved. This may have important implications in soil modelling and geotechnical/geological practice since many soils in nature (apart from tailings-type materials) may be of silt-size, which implies no noticeable particle breakage, but the critical state may deviate from the straight line as typically adopted by practicing engineers.

3.3.2 Behaviour of a broad range of tailings

Comparisons are now made across a wider range of tailings from different locations and parent rocks that have been reported in the literature, although the number of such detailed studies is very limited (Chang et al. 2011; Carrera et al. 2011; Bedin et al. 2012; Li 2017). Figure 14 gives the grading curves of these tailings. They are mainly silt to silty sand sized with D_{50} values ranging from 0.011 to 0.220 mm. The mineralogies of the various tailings are so diverse that they do not easily provide a basis for comparison, and so the following discussion will focus on grading. However, they are generally composed of low-plasticity or non-plastic material. There are four groups of materials: the gold tailing tested in this study and by Bedin et al. (2012), the iron tailings tested by Li (2017), the gold tailings tested by Chang et al. (2011), and the fluorite tailings tested by Carrera et al. (2011). The copper tailing tested by Li (2017) has an intermediate sandy silt grading between the two Brazilian gold tailings.

One key difference is that the gradings of the Stava fluorite tailing of Carrera et al. (2011) are of a rotating type where the gradings were changed artificially by adding increasing amounts of fines, while the other tailings were tested with "natural" in-situ gradings, so the gradings tend to translate with location in the lagoon and to be more poorly graded. The C_u values of most of the tailings are higher than 5 and the C_z values are between 1-3, so they might be considered as well-graded soils, but it can be seen from the grading curves that the major parts of these curves are fairly vertical, followed by long tails, which give these high C_u and C_z values, so in reality they are not really well-graded but relatively poorly graded. The sorting by sedimentation at different locations may give rise to these kinds of grading curves and it is possible that within the beach and lagoon the sedimentation of the coarser particles at any location occurs within a suspension of fines. In Figure 15, the compression indices C_c are plotted against D_{50} or C_u for different tailings. Within the scatter of the data, the compression index was found independent of D_{50}, but a possible trend of decreasing C_c was observed with increasing C_u. This finding is consistent with that of Altuhafi and Coop (2011), even though for a single type of tailing, for example the iron tailings tested by Li (2017), C_c actually increased with C_u, which indicates that C_u cannot be the only important factor, and effects of minerology and/or particle shape may be more significant. However, since the mineralogies and particle shapes of these tailings are complex, and very different between different tailings, no clear conclusion can be drawn about their effects.

Figure 16 shows the CSLs of the different tailings. Except for the iron tailing taken from the pond (PO) of a lagoon (Li, 2017), all the CSLs are curved, and are fairly flat at low to medium stresses but tending to be parallel to their corresponding 1D-NCLs at high stresses. The horizontal asymptotes of the CSLs of the different tailings vary significantly but the CSLs at high stresses are perhaps more similar than might have been expected given the wide range of gradings. For both the gold and iron tailings, the horizontal asymptote of the CSL for the silty tailing is above that for the sandy one, which is contrary to the findings of Carrera et al. (2011), perhaps because the former are for "natural" in-situ gradings. As Carrera et al. (2011) and Bedin et al. (2012) found, it is the location of this asymptote that controls full static liquefaction, although strong strain softening behaviour will still take place for undrained tests that reach the curved section of the CSL. The CSL of the PO iron tailing is straight and has no horizontal asymptote, while the CSLs of the gold and copper tailings do, even if the gradings are fairly similar, so particle sizes are clearly not the sole indicator of behaviour.

Figure 17 shows the relationship between the critical state angle of shearing resistance φ'_{cs} and D_{50} or D_F for the different tailings. Figure 17(a) shows that all the φ'_{cs} values for different tailings fall into a narrow range at about 33° ± 2°, which indicates that the particle sizes and mineralogies do not much affect φ'_{cs}. In Figure 17(b), within the data scatter, there is a decreasing trend of φ'_{cs} value with the increase of fractal dimension D_L, which is consistent with the results of Vallejo et al (2017).

Figure 18(a) shows the SBS of different tailings using the same normalisation as in Figure 8. The gold tailings data from this paper are repeated here but unfortunately a SBS is not available for the coarser tailing of Bedin et al. (2012). The SBS has a variety of sizes and shapes, but overall, as the tailings get coarser, the size increases and the peak on the wet (right) side of the CSL becomes more pronounced as the SBS becomes more like that of a sand. Figure 18(b) shows the relationship between the spacing of the isotropic NCL and CSL expressed as a stress ratio and the D_{50} for the different tailings; the isotropic NCLs are not highlighted, but are at the intercept of the SBS with the p'/p'_{cs} axis. It is clear that the ratio tends towards higher values with the increase of mean particle size. For iron tailings (Li, 2017), the pond (PO) material has a stress ratio of about 2.7, and the ratio for the gold tailing is about 2.2, which are both similar to the values expected for clays, but these are non-plastic materials. For the copper tailing (Li, 2017), even if it has a similar grading to the middle beach (MB) iron tailing, the stress ratio of about 3.3 is higher, again indicating that the mineralogies may be also important.

The horizontal asymptote of the CSL is assumed to define the specific volume above which full static liquefaction must occur on undrained loading. These values (v_{liq}) are plotted along with maximum and minimum specific volumes (v_{max} & v_{min}) against the fines content (f_c) (Figure 19a). Since the standards ASTM D 4253 and D 4254 (2002) are not suitable to measure the maximum and minimum void ratio for a sand with f_c higher than 10%, the v_{max} and v_{min} here were obtained from the initial specific volumes of the loosest and of the densest samples that could be prepared in the tests, similarly to Carrera et al. (2011). Different groups of tailings are labelled with different symbols. In the results of Bedin et al. (2012), it is unusual that the specific volumes of all samples lie above v_{liq}, which means that the coarse gold tailing is extremely susceptible to liquefaction. Figure 19(b) shows same data plotted against D_{50}, but this also seems not to affect the relative position of v_{liq} consistently. Lade and Yamamuro (1997) reported a decrease in resistance to liquefaction with the increasing f_c, and that the liquefaction boundary moves closer to e_{min} (here v_{min}) with the increase of f_c, up to 50%. For comparisons, approximate trend lines for v_{max}, v_{min} and v_{liq} are added in Figures 19(a) and 19(b), based on the data points of all the tailings except the gold tailing tested by Bedin et al. (2012), which seem to be unusual compared with other tailings. As shown in Figure 13, the “natural” in-situ gradings of the tailings tend to translate rather than rotate, and so analysing them in terms of f_c may be misleading and it seems more reasonable to study them in terms of D_{50}. It can be seen that the boundary specific volumes for different tailings do not change that much, even if the D_{50} values range from 0.011 to 0.220 mm, but they do slightly decrease and increase again with increasing D_{50} or f_c, which is consistent with Lade and Yamamuro (1997). The v_{liq} locations seem quite scattered but overall they are reasonably constant in between the v_{max} and v_{min}, in contrast to the findings of Lade and Yamamuro (1997). The implication of this is that in general neither the finer pond tailings nor the coarser upper beach would be more susceptible to liquefaction. However, for individual tailings, for example the iron tailings of Li (2017) or the fluorite tailings tested by Carrera et al. (2011), the variation of susceptibility with grading may be different. Again, the complex mineralogies, particle shapes and also the different gradings types may give rise to these different behaviours and scatter.

4. Conclusions

A detailed study of the mechanics of a gold tailing from Brazil found that the one-dimensional compression paths converged slowly and at 7MPa vertical stress a unique NCL could still not be defined and so the material might be said to be slightly transitional or slowly convergent. Different sample preparation methods gave very similar rates of convergence, and so they had little effect on the compression behaviour. At 20MPa vertical stress level, the compression curves finally converged. In shearing a unique CSL can be defined at much lower stress levels than were required to bring about convergence in compression, which implies that the differences of initial specific volume that can only arise from differences of fabric are more easily erased by shearing than by compression. Through comparing the elastic shear moduli and also the critical states of samples prepared by different methods, it was found that any fabric effects from the sample preparation method were negligible at both smaller and larger strain levels.

Comparing the results with the study of Bedin et al. (2012) on a coarser grading of the same tailing, it is found that the 1D-NCL is much easier to reach for the sandy tailing, but that at higher stresses the locations of the 1D-NCLs of the two tailings were surprisingly similar given that sandy material undergoes significant breakage but the silty one tested here does not. The CSLs for the silty and sandy tailings were also found to be quite similar, although the horizontal asymptote for the silty tailing is above that for the sandy one. Combining this with its denser initial states, this tailing would therefore be much less susceptible to liquefaction.

Comparing a variety of different tailings, it is found that neither the D_{50} nor C_u values can be used to characterise the compression indices very successfully, but the C_u has a clearer influence. Grading is clearly not the only important factor, and the effects of minerology and particle shape must also be significant. The horizontal asymptotes of the CSLs of the different tailings vary significantly but the CSL locations at high stresses are quite similar, considering the wide variability in grading. Despite the differences of grading and mineralogy all the φ'_{cs} values of different tailings fall into a narrow range at 33° ± 2°. The size of the state boundary surface, as quantified with the stress ratio between the isotropic NCL and the CSL, tends towards higher values with the increase of D_{50}.

The boundary specific volumes for different tailings do not change that much, given the large grading differences, but they do slightly decrease and increase again with the increasing f_c, which is consistent with Lade and Yamamuro (1997). The values of the asymptote of the CSL which defines the specific volume above which full liquefaction must occur, v_{liq}, are quite scattered but are generally reasonably constant in between v_{max} and v_{min}, with the increase of either f_c or D_{50}, in contrast to the findings of Lade and Yamamuro (1997). The implication of this is that in general neither the pond nor the upper beach is more susceptible to liquefaction, but for individual tailings the trends may vary.

Acknowledgements

The work described in this paper was fully supported by a grant from the Research Grants Council of the Hong Kong Special Administrative Region, China (project no. CityU 112813). The first author would like to thank Mr. Liu Haifeng from the Institute of Rock and Soil Mechanics, Chinese Academy of Sciences, for his help in the XRD tests.

Notations

1D-NCL one-dimensional normal compression line
C_c compression index
CSL critical state line
C_u coefficient of uniformity
C_z coefficient of curvature
D_{50} mean particle size
D_F fractal dimension
e void ratio
f_c fines content
G shear modulus
G_s specific gravity of soil particles
m gradient of v_{final} : $v_{initial}$ data
M stress ratio at critical state
NCL normal compression line
p' mean effective stress
p_0' mean effective stress the sample sheared from.
q deviatoric stress
SBS state boundary surface
SSL steady state line

v specific volume

v_i initial specific volume

v_{liq} horizontal asymptote of the CSL

v_{max} maximum specific volume

v_{min} minimum specific volume

w_i initial water content

Δu change of pore water pressure

σ'_{vmax} maximum vertical stress

Φ diameter of sample

φ'_{cs} angle of shearing resistance at critical state

ψ state parameter

References

Altuhafi, F. N., & Coop, M. R. (2011). Changes to particle characteristics associated with the compression of sands. Géotechnique, 61(6), 459-471.

ASTM, (2002). Annual book of ASTM standards.

Bedin, J., Schnaid, F., da Fonseca, A. V., & Costa Filho, L. D. M. (2012). Gold tailings liquefaction under critical state soil mechanics. Géotechnique, 62(3), 263-267.

Bishop, A. W., & Wesley, L. D. (1975). A hydraulic triaxial apparatus for controlled stress path testing. Géotechnique, 25(4), 657-670.

Carrera, A., Coop, M., & Lancellotta, R. (2011). Influence of grading on the mechanical behaviour of Stava tailings. Géotechnique, 61(11), 935-946.

Chandler, R. J., & Tosatti, G. (1995). The Stava tailings dams failure, Italy, July 1985. Proceedings of the ICE-Geotechnical Engineering, 113(2), 67-79.

Chang, N, Heymann, G. & Clayton, C. (2011). The effect of fabric on the behaviour of gold tailings. Géotechnique, 61(3), 187-197.

Coop, M. R., & Lee, I. K. (1993). The behaviour of granular soils at elevated stresses. Predictive soil mechanics Edited by GT Houlsby and AN Schofield. Thomas Telford, London, UK, 186-198.

Coop, M.R. (2015) Limitations of a Critical State Framework Applied to the Behaviour of Natural and "Transitional" Soils. 6th Intl Symp. on Deformation Characteristics of Geomaterials, Buenos Aires, 115-155.

Fourie, A. B., Blight, G. E., & Papageorgiou, G. (2001). Static liquefaction as a possible explanation for the Merriespruit tailings dam failure. Canadian Geotechnical Journal, 38(4), 707-719.

Gens, A., & Alonso, E. E. (2006). Aznalcóllar dam failure. Part 2: Stability conditions and failure mechanism. Géotechnique, 56(3), 185-202.

Hyslip, J. P., & Vallejo, L. E. (1997). Fractal analysis of the roughness and size distribution of granular materials. Engineering geology, 48(3-4), 231-244.

Jovičić, V., & Coop, M. P. (1998). The measurement of stiffness anisotropy in clays with bender element tests in the triaxial apparatus. Geotech. Test. J., 21(1), 3-10.

Lade, P. V., & Yamamuro, J. A. (1997). Effects of nonplastic fines on static liquefaction of sands. Canadian Geotechnical Journal, 34(6), 918-928.

Li, W. (2017). The mechanical behaviour of tailings. PhD Thesis, City University of Hong Kong.

Li, W., & Senetakis, K. (2017). Dynamic shear modulus of three reconstituted soils from Panzhihua iron tailing dam. Journal of Geo-engineering, 12(3), 129-135.

Martins, F. B., Bressani, L. A., Coop, M. R., & Bica, A. V. D. (2001). Some aspects of the compressibility behaviour of a clayey sand. Canadian Geotechnical Journal, 38(6), 1177-1186.

Okewale, I.A. & Coop, M.R. (2017). A study of the effects of weathering on soils derived from decomposed volcanic rocks Engineering Geology, 222, 53-71.

Okusa, S. & Anma, S. (1980). Slope failures and tailings dam damage in the 1978 Izu-Ohshima-Kinkai earthquake. Engineering Geology, 16(3-4), 195-224.

Ozer, A.T. & Bromwell L.G. (2012). Stability assessment of an earth dam on silt/clay tailings foundation: A case study. Engineering Geology, 151, 89-99.

Payan, M., Khoshghalb, A., Senetakis, K., & Khalili, N. (2016). Effect of particle shape and validity of Gmax models for sand: A critical review and a new expression. Computers and Geotechnics, 72, 28-41.

Ponzoni, E., Nocilla, A., Coop, M. R., & Colleselli, F. (2014). Identification and quantification of transitional modes of behaviour in the Sediments of Venice Lagoon. Géotechnique, 64(9), 694-708.

Rocchi, I., & Coop, M.R. (2014). Experimental Accuracy of the Initial Specific Volume. Geotechnical Testing Journal, 37(1), 169-175.

Rocchi, I., & Coop, M.R. (2015). The effects of weathering on the physical and mechanical properties of a granitic saprolite. Géotechnique, 65(6), 482-493.

Roscoe, K. H., Schofield, A., & Wroth, C. P. (1958). On the yielding of soils. Géotechnique, 8(1), 22-53.

Roscoe, K., & Burland, J. B. (1968). On the generalized stress-strain behaviour of 'wet' clay. Engineering Plasticity, 535-609.

Schnaid, F., Bedin, J., Viana da Fonseca, A. J. P., & de Moura Costa Filho, L. (2013). Stiffness and strength governing the static liquefaction of tailings. Journal of Geotechnical and Geoenvironmental Engineering, 139(12), 2136-2144.

Tyler, S. W., & Wheatcraft, S. W. (1992). Fractal scaling of soil particle-size distributions: analysis and limitations. Soil Science Society of America Journal, 56(2), 362-369.

Vallejo, L. E. (1996). Fractal analysis of the fabric changes in a consolidating clay. Engineering Geology, 43(4), 281-290.

Vallejo, L. E., Espitia, J. M., & Caicedo, B. (2017). The influence of the fractal particle size distribution on the mobility of dry granular materials. In EPJ Web of Conferences, 140, 03032.

Wise Uranium Project (WISE). (2014). Chronology of Major Tailings Dam Failures, website: http://www.wise-uranium.org/mdaf.html.

Xu, L., & Coop, M. R. (2016). The mechanics of a saturated silty loess with a transitional mode. Géotechnique, 1-16.

Zandarin, M.T., Oldecop, L.A., Rodriguez, R. & Zabala F. (2009). The role of capillary water in the stability of tailing dams. Engineering Geology, 105(1-2), 108-118.

Zhang, Q., Yin, G., Wei, Z., Fan, X., Wang, W. & Nie, W. (2015). An experimental study of the mechanical features of layered structures in dam tailings from macroscopic and microscopic points of view. Engineering Geology, 195, 142-154.

LIST OF TABLES

LIST OF FIGURES

Table 1: Characteristics of different types of tailings.

Tailings type	D_{50} (mm)	C_u	C_z	G_s	C_c	φ'_{cs} (°)
Gold (in this study)	0.011	7.3	1.4	2.89	0.30	34.8
Gold (Bedin et al., 2012)	0.065	7.0	2.3	2.89-3.20	0.44	33.0
Gold-UB (Chang et al., 2011)	0.095	24.1	2.2	2.72	0.11	31.1
Gold-MB (Chang et al., 2011)	0.053	10.5	0.8	2.69	0.30	33.6
Gold-PO (Chang et al., 2011)	0.006	2.6	1.6	2.75	0.49	31.5
Copper (Li, 2017)	0.031	5.1	1.5	3.75	0.22	35.2
Iron-UB (Li, 2017)	0.22	10.4	2.6	3.37	0.38	34.6
Iron-MB (Li, 2017)	0.035	10	1.1	3.14	0.32	33.7
Iron-PO (Li, 2017)	0.023	6.7	2.2	3.11	0.19	34.8
Fluorite-sand (Carrera et al., 2011)	0.180	2.5	1.1	2.72	0.19	35.0
Fluorite-9010 (Carrera et al., 2011)	0.169	2.7	0.8	-	0.18	-
Fluorite-7030 (Carrera et al., 2011)	0.125	9.3	1.8	-	0.11	-
Fluorite-5050 (Carrera et al., 2011)	0.075	11.5	1.0	-	0.10	-
Fluorite-3070 (Carrera et al., 2011)	0.044	10.0	1.1	-	0.09	-
Fluorite-silt (Carrera et al., 2011)	0.026	9.7	2.6	2.83	0.10	33.0

Note: D_{50} mean particle size. C_u and C_z coefficient of uniformity and curvature. G_s specific gravity. C_c compression index. φ'_{cs} angle of shearing resistance at critical state. UB, MB and PO tailings taken from the upper beach, middle beach and pond of a tailings dam respectively. 9010 90% sand and 10% fines. 7030, 5050 and 3070 similar with 9010 but different sand and fines contents.

Table 2: Summary of the one-dimensional compression tests.

Test no.	Φ (mm)	Preparation method	w_i (%)	v_i	σ'_{vmax} (kPa)
1	50		19	2.02	7,100
2	50		19	2.01	7,100
3	50		19	1.82	7,100
4	50		20	2.31	7,100
5	50		20	1.75	7,100
6	50	wet compaction	20	1.74	7,100
7	50		25	1.80	7,100
8	50		25	1.79	7,100
9	30		19	2.14	19,800
10	30		20	1.69	19,800
11	50		0	2.27	7,100
12	50		0	2.31	7,100
13	50		0	2.03	7,100
14	50		0	2.03	7,100
15	50		0	2.01	7,100
16	50	dry compaction	0	2.02	7,100
17	50		0	1.99	7,100
18	50		0	1.87	7,100
19	50		0	1.84	7,100
20	50		0	1.96	7,100
21	50		60	2.36	7,100
22	50		54	2.05	7,100
23	50		53	2.09	7,100
24	50		49	2.10	7,100
25	50	slurry	47	2.05	7,100
26	50		47	2.04	7,100
27	50		43	1.96	7,100
28	50		38	1.93	7,100

Note: Φ diameter of sample. w_i and v_i initial water content and specific volume. σ'_{vmax} maximum vertical stress.

Table 3: Summary of the triaxial tests.

Test No.	Shearing type	Equipment	Preparation method	w_i (%)	v_i	p_0' (kPa)
1	CIU	Conv.	wet compaction	20	1.78	200
2	CIU	Conv.	wet compaction	20	1.82	400
3	CIU	Conv.	wet compaction	20	1.85	300
4	CIU	Conv.	wet compaction	20	1.91	100
5	CIU	Conv.	wet compaction	20	1.73	200
6	CIU	Conv.	wet compaction	20	1.73	100
7	CIU	Conv.	wet compaction	20	1.91	100
8	CIU	Conv.	wet compaction	20	1.94	400
9	CIU	Conv.	wet compaction	20	1.95	100
10	CIU	Conv.	wet compaction	20	1.97	400
11	CIU	Conv.	wet compaction	10	1.99	700
12	CIU	Conv.	wet compaction	10	2.01	600
13	CIU	Conv.	wet compaction	10	1.95	600
14	CIU	Conv.	wet compaction	10	2.06	50
15	CIU	Conv.	wet compaction	10	2.08	20
16	CIU	Conv.	wet compaction	10	2.08	20
17	CIU	Conv.	wet compaction	5	2.05	700
18	CIU	Conv.	wet compaction	5	2.03	50
19	CIU	Conv.	wet compaction	5	2.02	50
20	CIU	Conv.	slurry	40	1.91	50
21	CIU	Conv.	slurry	45	1.93	50
22	CID	Conv.	wet compaction	20	1.78	200
23	CID	Conv.	wet compaction	20	1.74	300
24	CID	Conv.	wet compaction	20	1.94	300
25	CID	Conv.	wet compaction	20	1.89	400
26	CID	Conv.	wet compaction	10	2.06	50
27	CID	Conv.	wet compaction	10	1.95	50
28	CID	Conv.	wet compaction	10	2.07	20
29	CID	Conv.	wet compaction	5	1.98	400
30	CID	Conv.	dry compaction	0	1.93	50
31	CIU	HP	wet compaction	20	1.68	6,000
32	CID	HP	wet compaction	10	1.99	6,000

Note: CIU isotropically consolidated undrained test. CID isotropically consolidated drained test. Conv. conventional apparatus. HP test conducted with high pressure triaxial apparatus. v_i and w_i initial specific volume and water content. p_0' mean effective stress the sample sheared from.

Table 4: Summary of bender element tests.

Test no.	Preparation method	v_i	Dry/Sat	G_{vh}	G_{hh}	G_{hv}
S_sat_1	slurry	1.95	Sat	●	●	●
C-sat_1	compaction	2.01	Sat	●	●	●
C_sat_2	compaction	1.95	Sat	●	-	-
C_dry_1	compaction	1.98	Dry	●	-	-
C_dry_2	compaction	1.91	Dry	●	-	-
C_dry_3	compaction	2.14	Dry	●	-	-

Note: S and C slurry and compaction. Sat saturated. v_i initial specific volume.

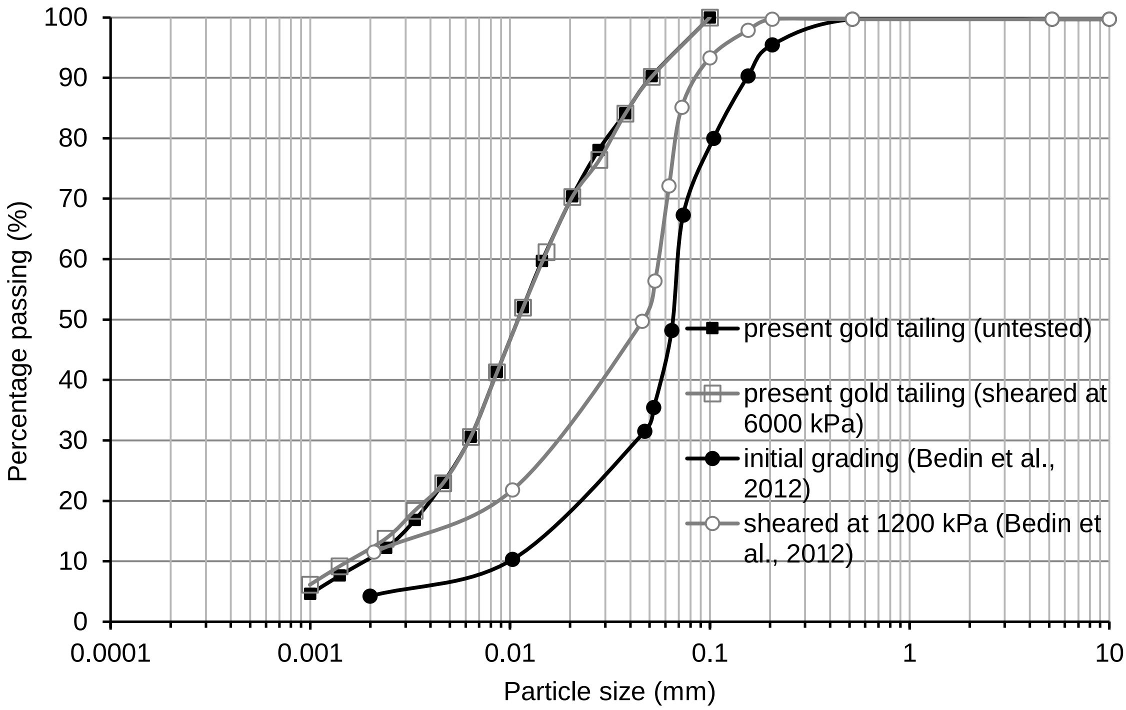

Figure 1: Particle size distributions of the present and Bedin's gold tailings.

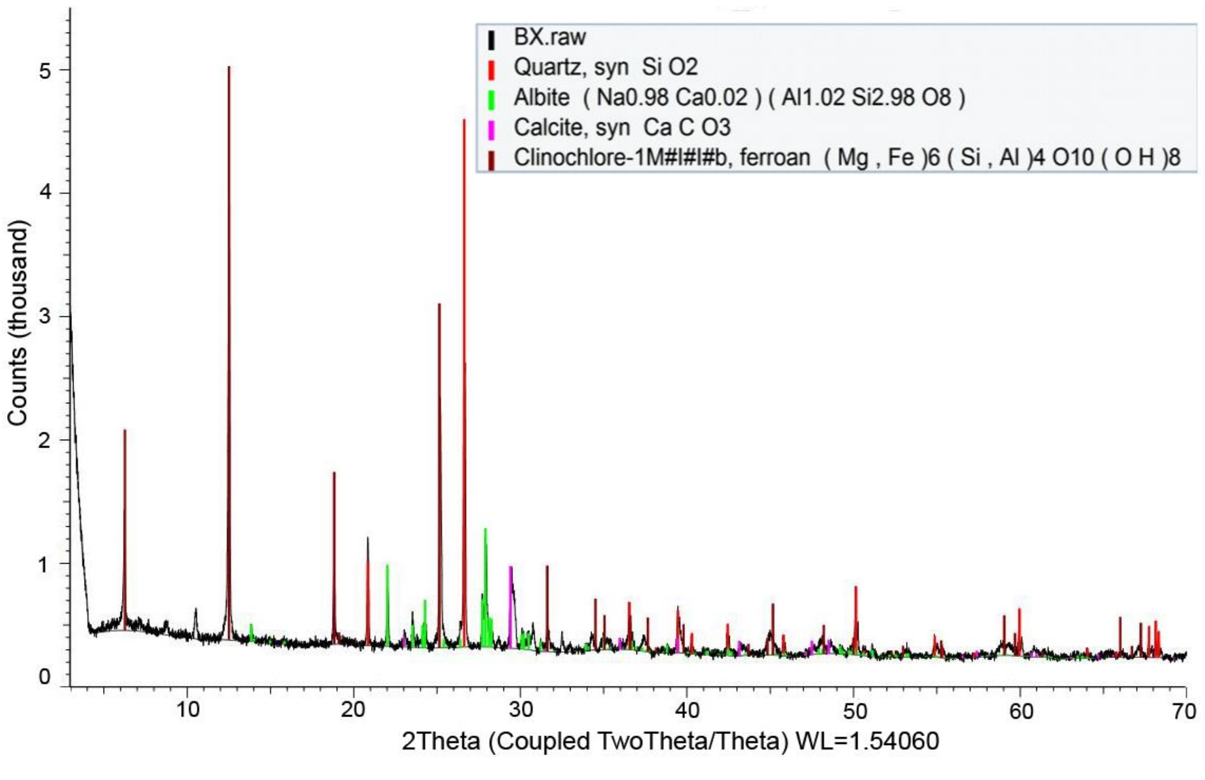

Figure 2: XRD analysis quantifying the mineral composition of the gold tailing.

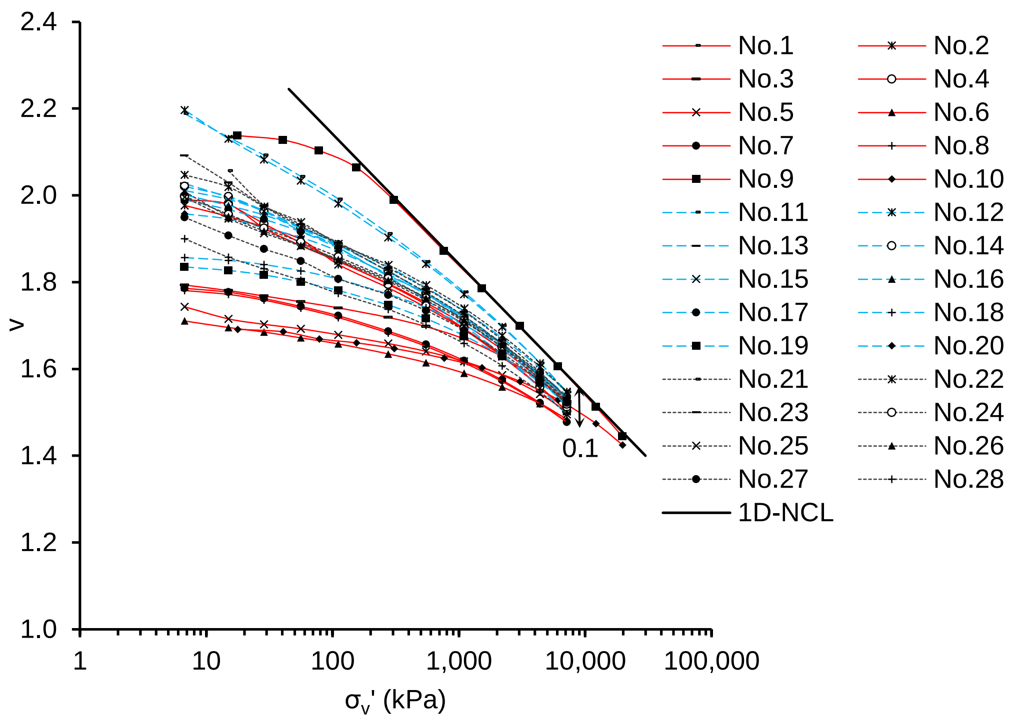

Figure 3: One-dimensional compression behaviour of the gold tailing.

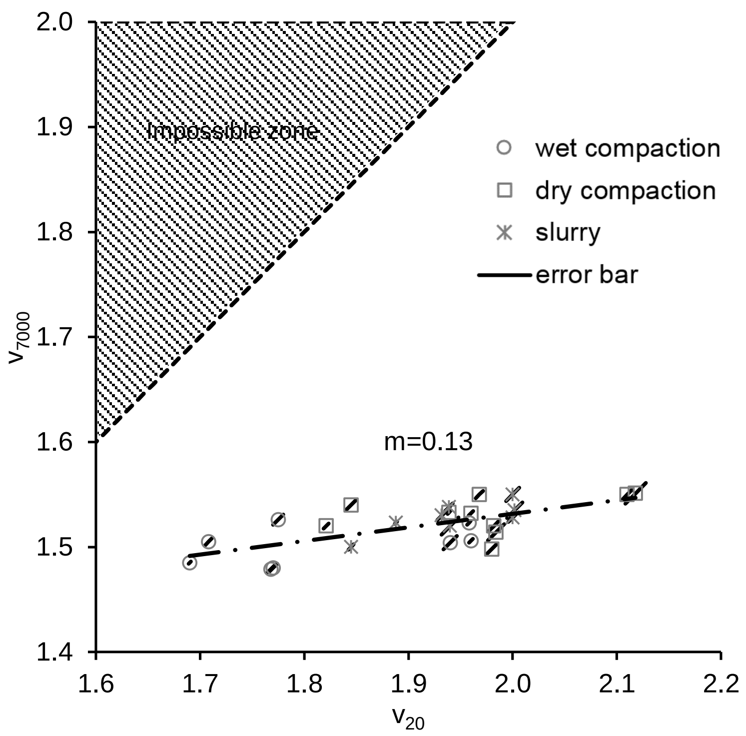

Figure 4: Calculation of m values for the tests with a maximum vertical stress of 7 MPa.

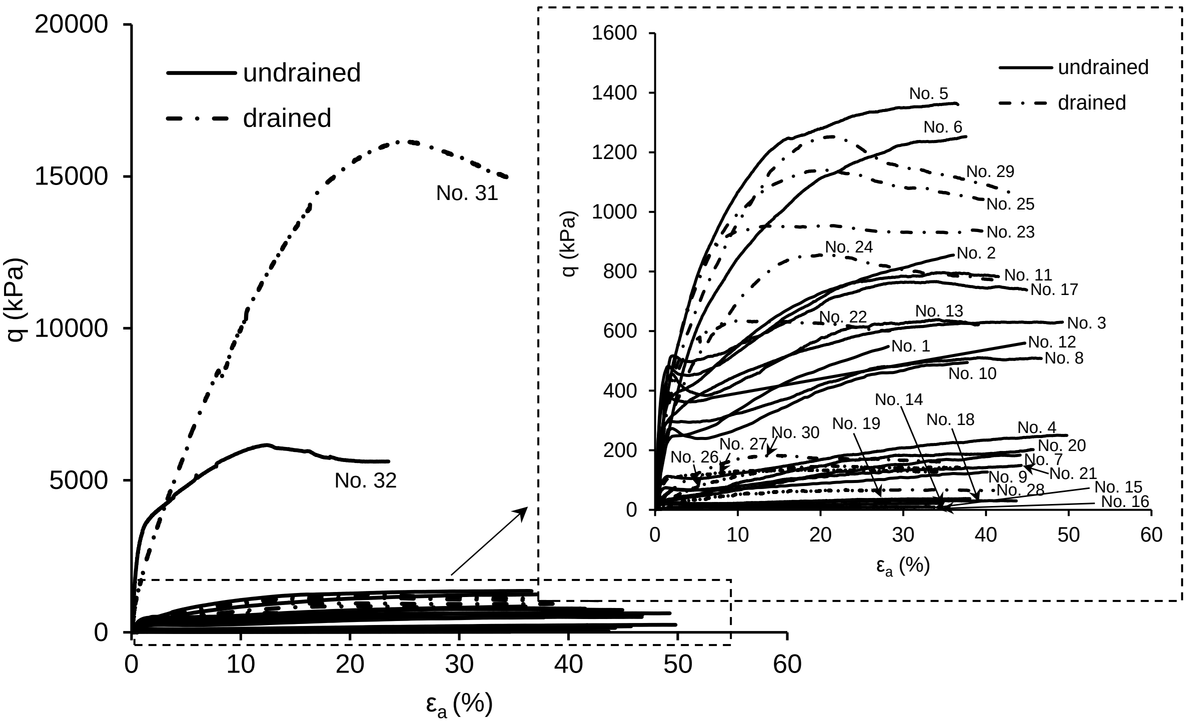

undrained
drained
No. 31
No. 32
q (kPa)
εa (%)
No. 5
No. 6
No. 29
No. 25
No. 23
No. 24
No. 2
No. 11
No. 17
No. 22
No. 13
No. 3
No. 1
No. 12
No. 8
No. 10
No. 14
No. 19
No. 18
No. 4
No. 30
No. 20
No. 27
No. 7
No. 26
No. 21
No. 9
No. 28
No. 15
No. 16

(a)

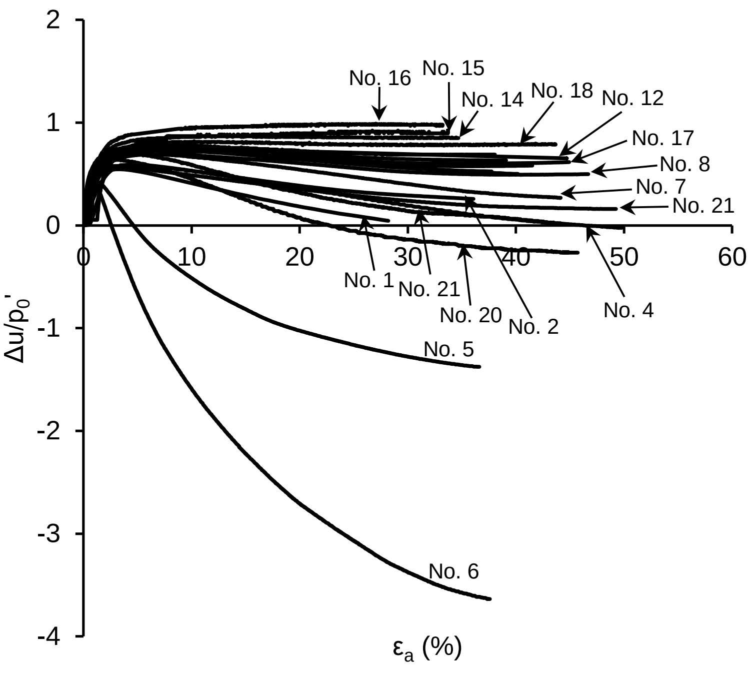

Δu/p0'
εa (%)
No. 16
No. 15
No. 14
No. 18
No. 12
No. 17
No. 8
No. 7
No. 21
No. 1
No. 21
No. 20
No. 2
No. 4
No. 5
No. 6

(b)

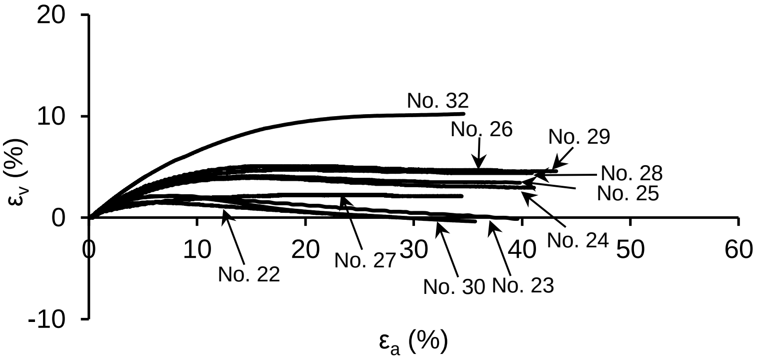

(c)

Figure 5: Triaxial test data of the gold tailing: (a) stress-strain data, (b) change of pore water pressure, and (c) volumetric strain.

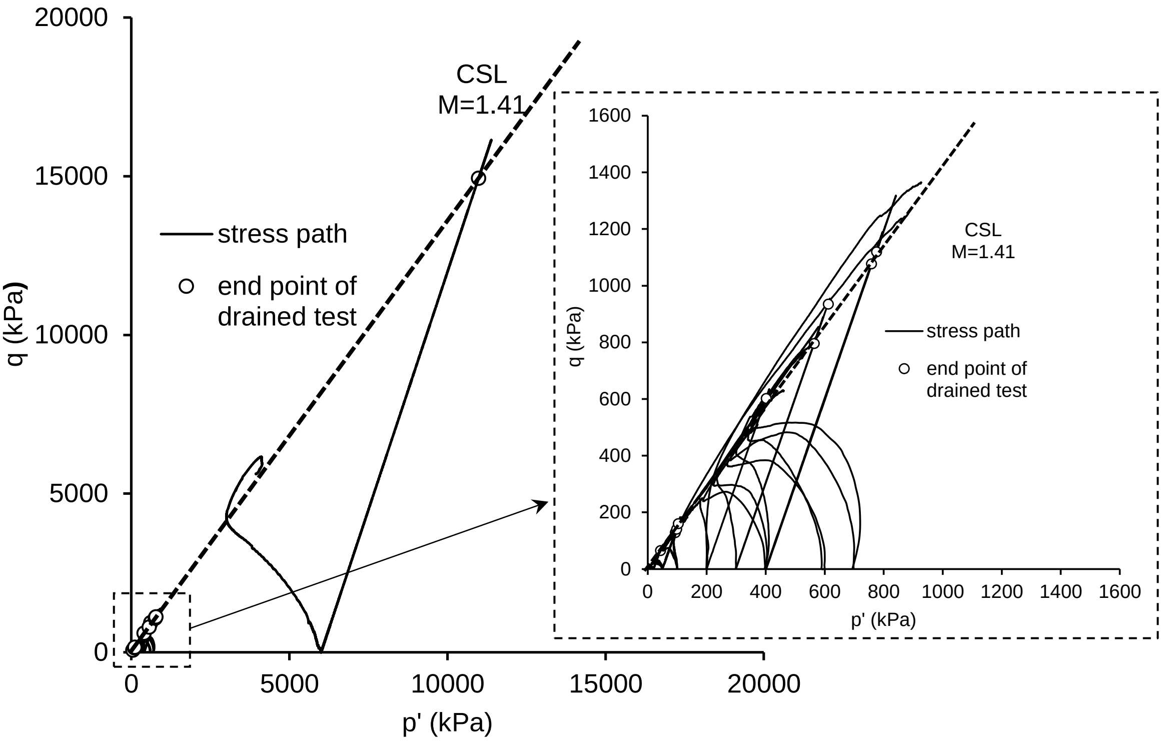

(a)

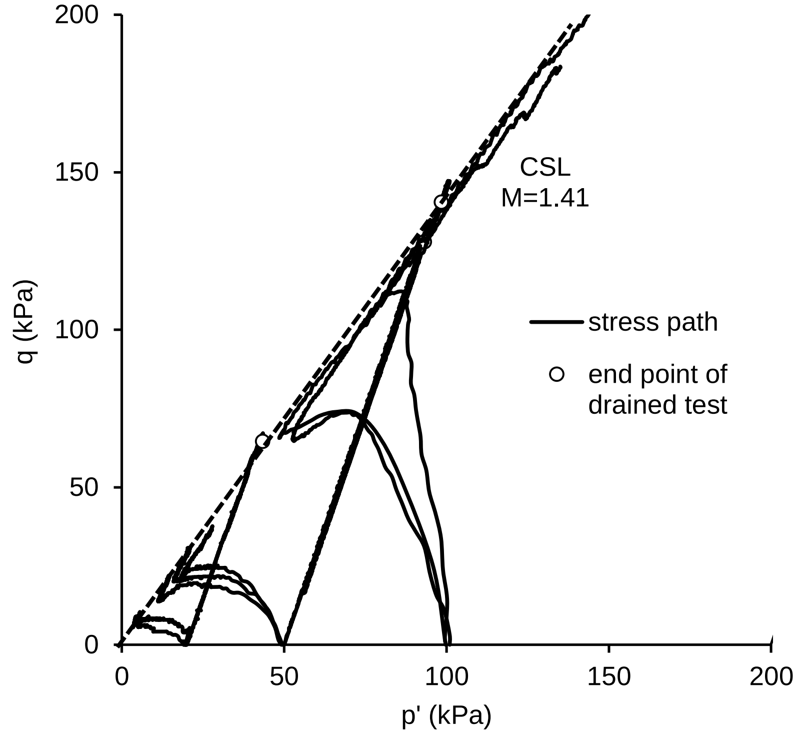

(b)

Figure 6: Stress paths and CSL in the q: p' plane: (a) all stress paths, and (b) expanded scale for p_0' less than 200 kPa.

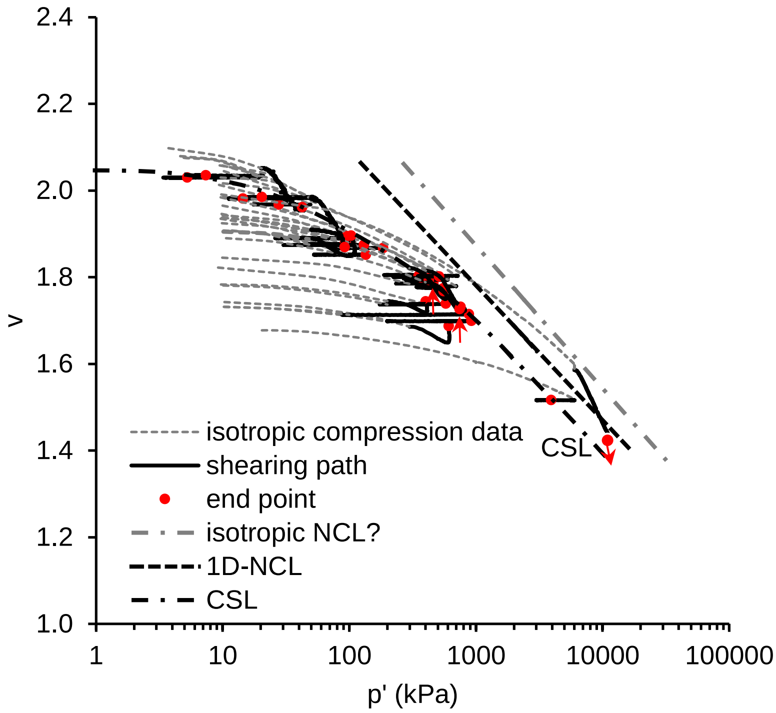

Figure 7: CSL together with 1D-NCL & estimated isotropic NCL in the volumetric plane.

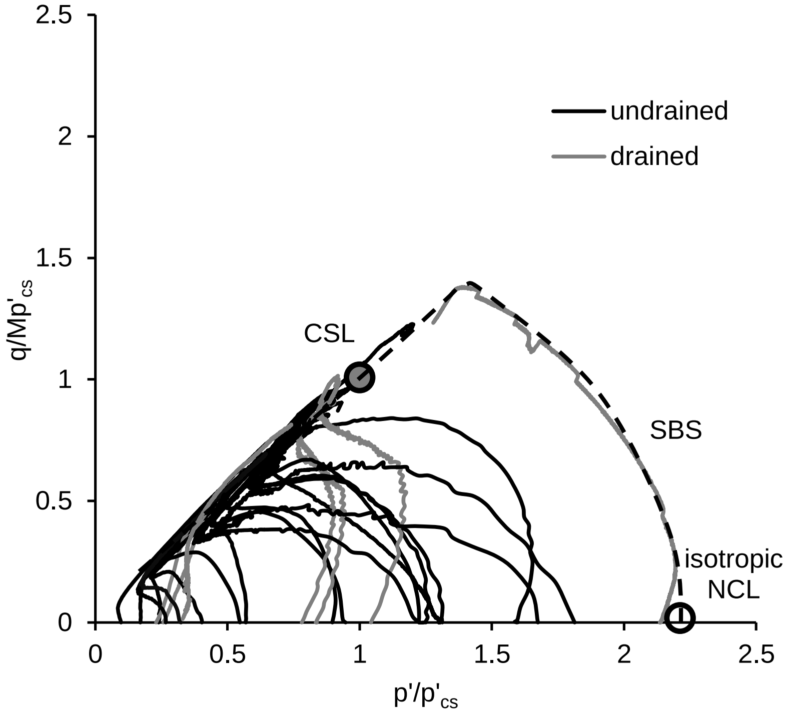

Figure 8: Normalised stress paths of the gold tailings.

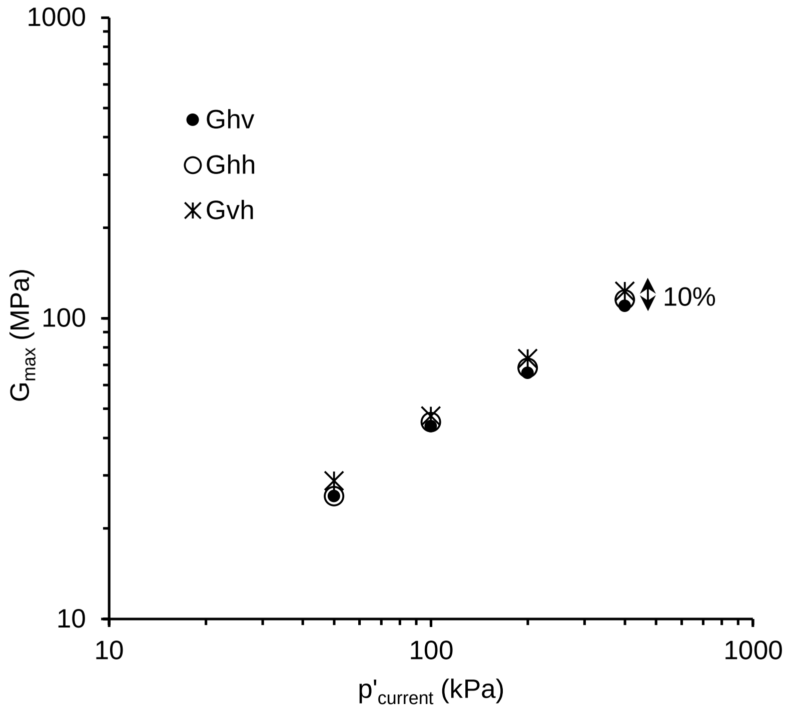

(a)

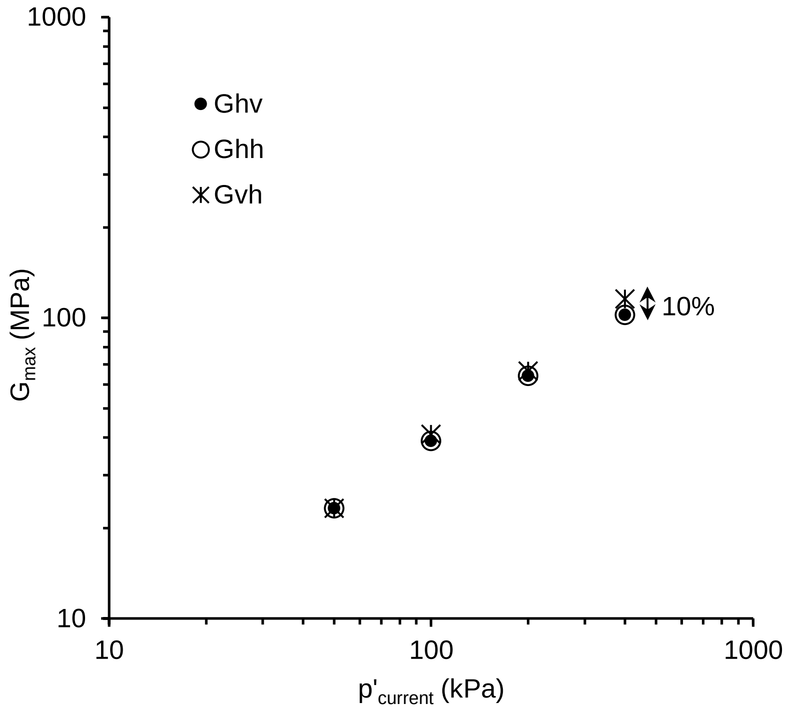

(b)

Figure 9: Small-strain shear modulus against the mean effective confining pressure: (a) a slurry sample and (b) a dry compacted sample.

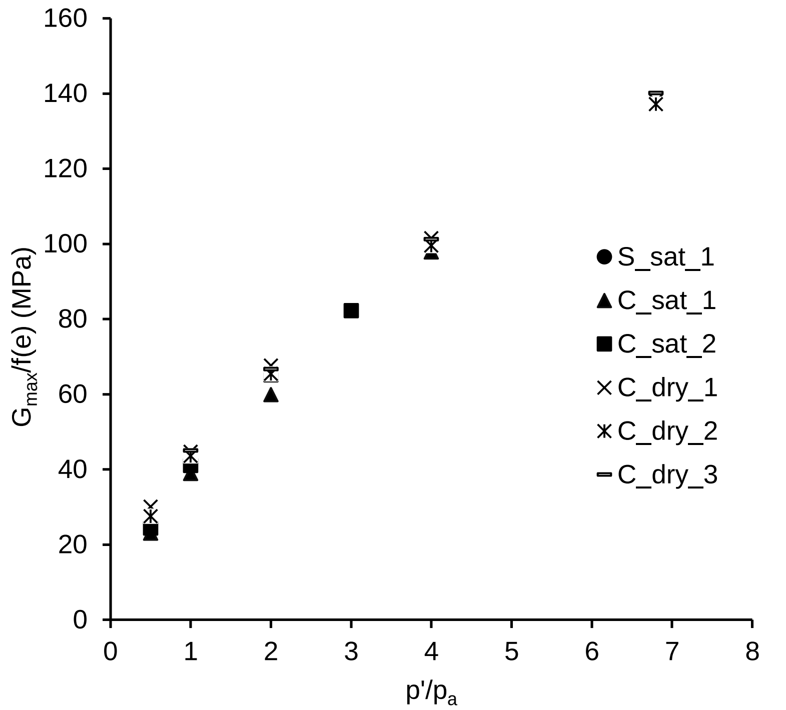

Figure 10: Normalized shear modulus (G_{vh}) comparing samples prepared with different preparation methods.

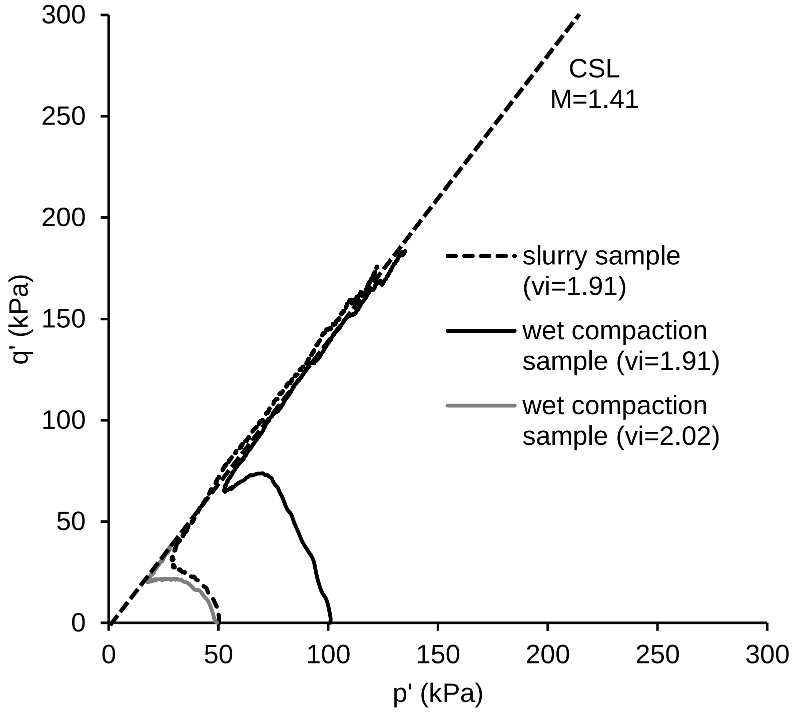

(a)

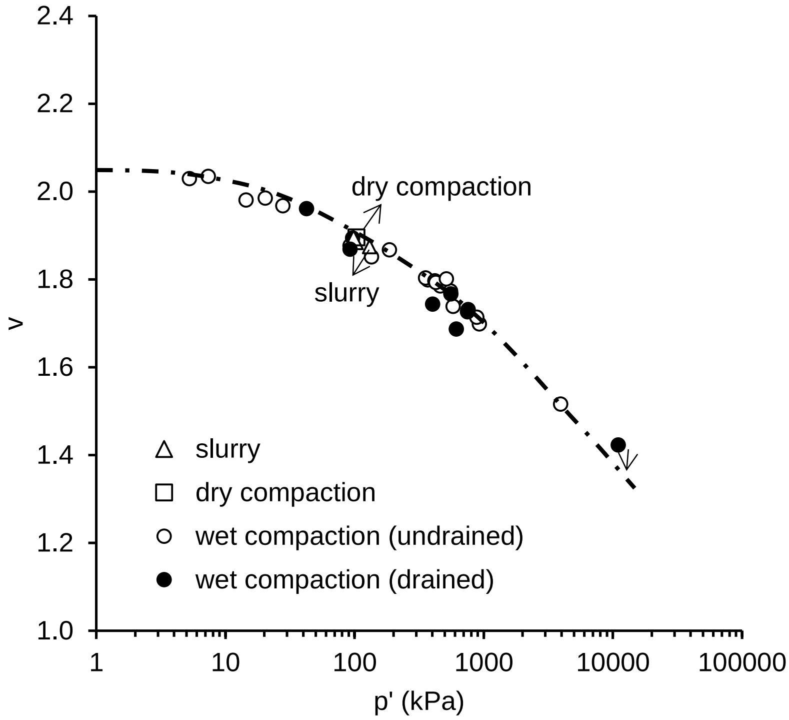

(b)

Figure 11: Fabric effects from different preparation methods on: (a) stress paths and (b) critical states.

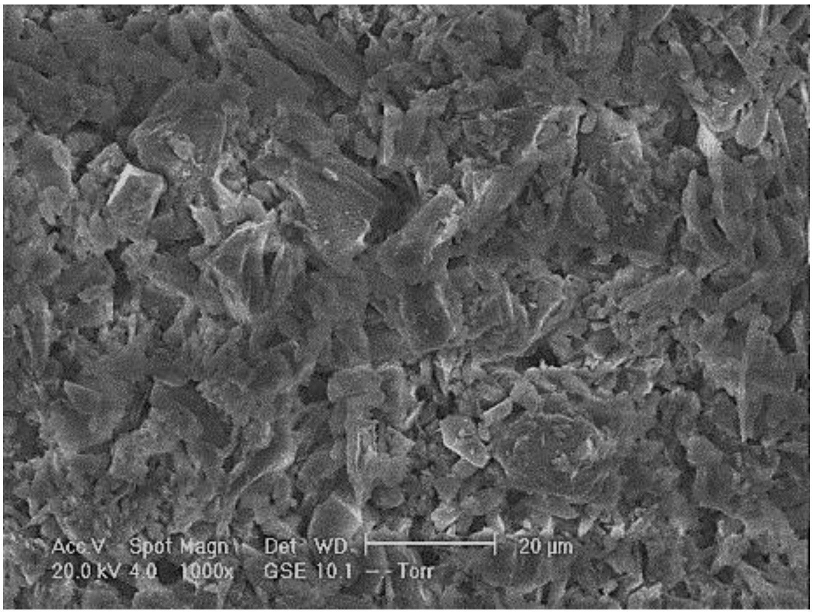

(a)

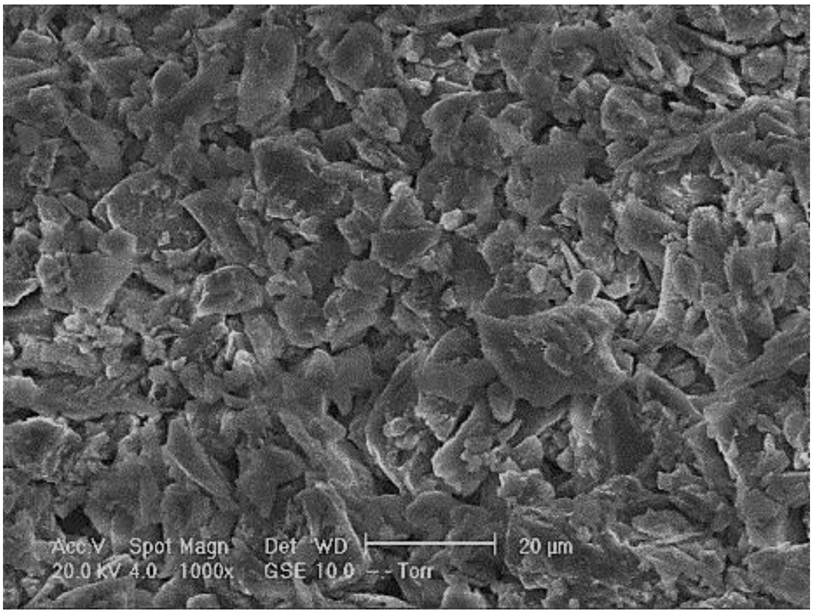

(b)

Figure 12: SEM pictures of: (a) a slurry sample and (b) a wet compacted sample.

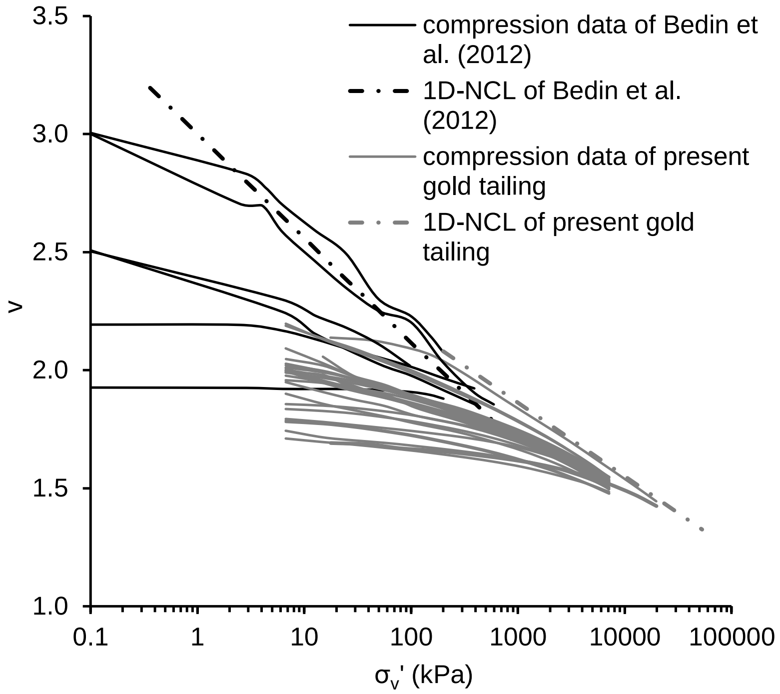

(a)

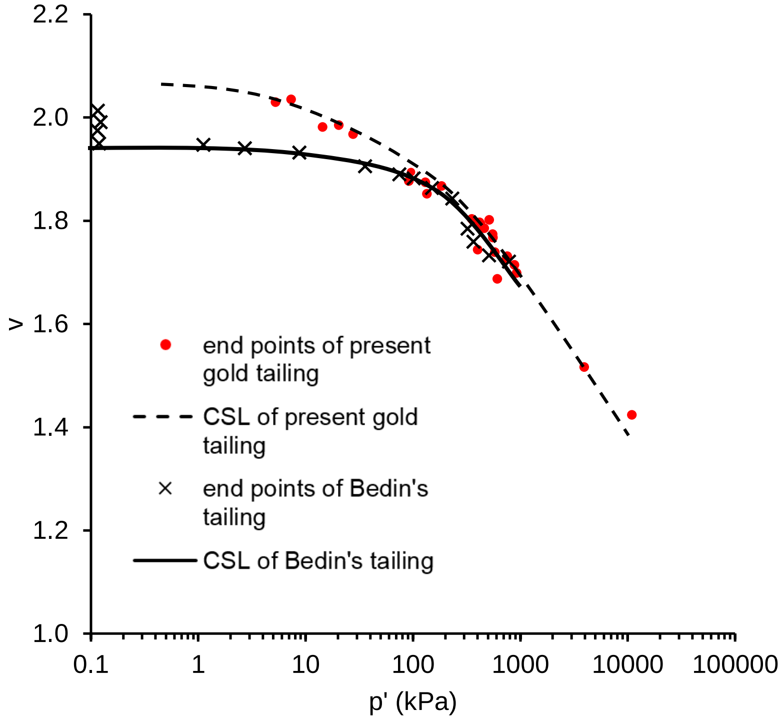

(b)

Figure 13: Comparisons of the two Brazilian gold tailings: (a) 1D-NCLs and (b) CSLs.

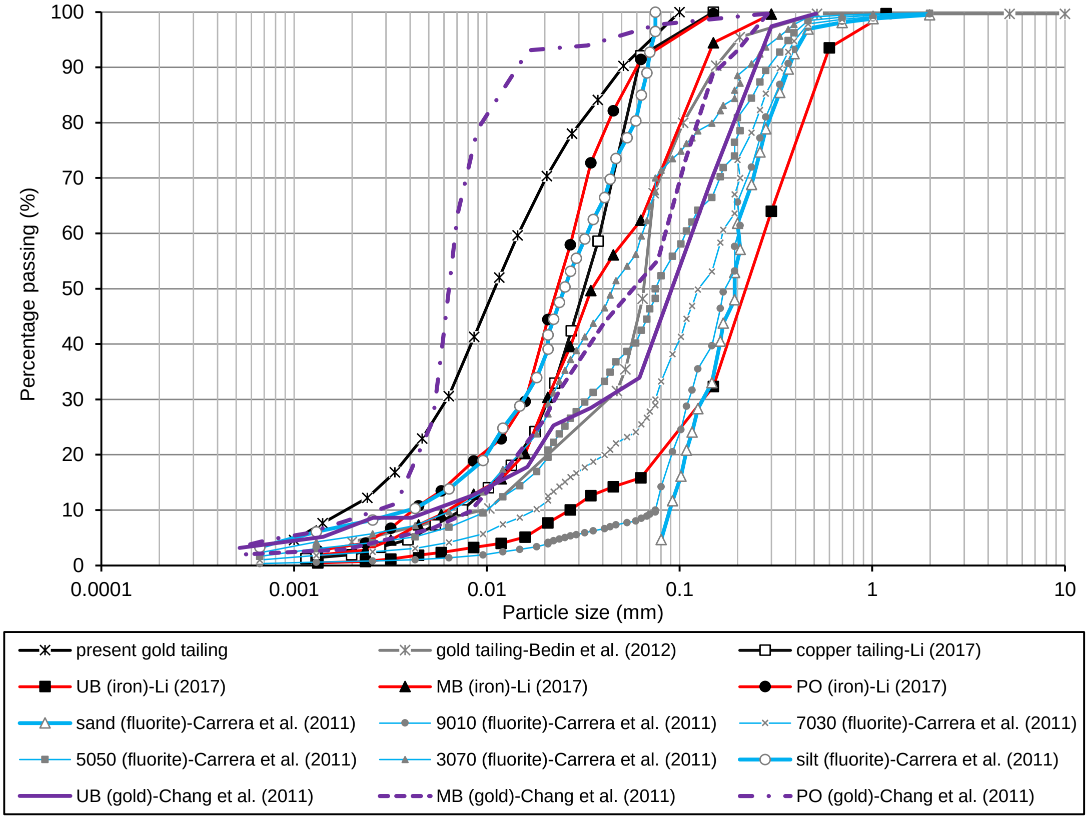

Figure 14: Gradings curves of the present gold tailing together with the data of Chang et al. (2011); Carrera et al. (2011); Bedin et al. (2012) and Li (2017).

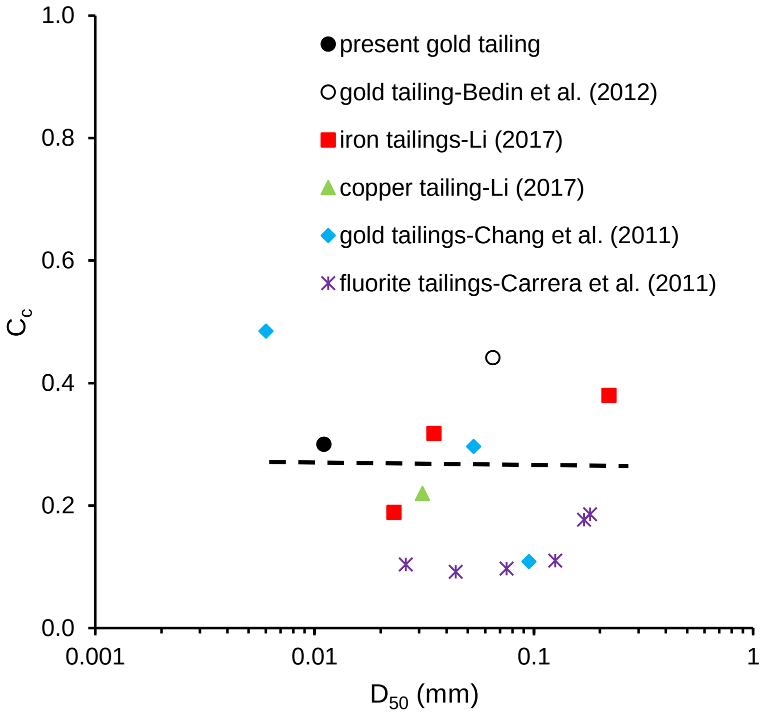

(a)

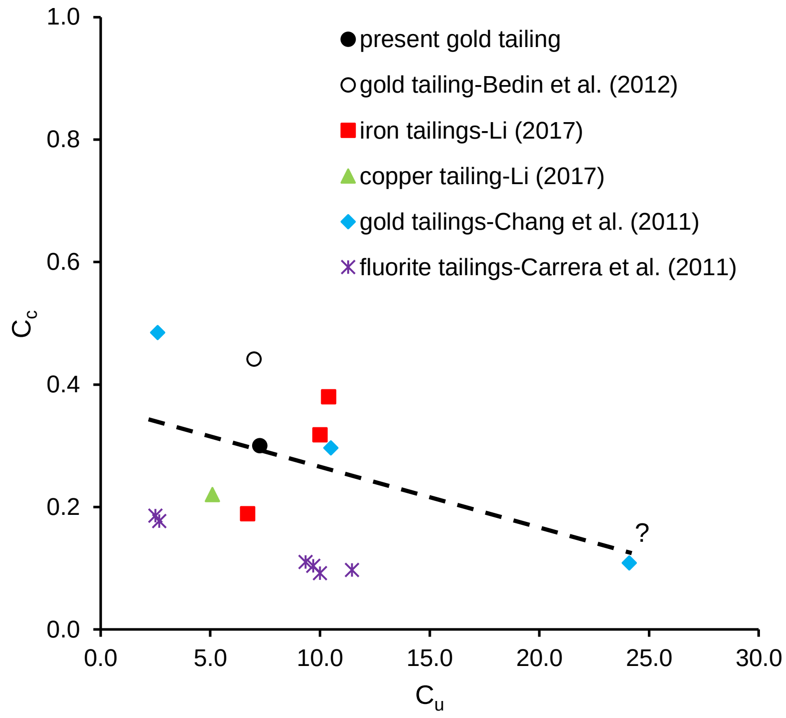

(b)

Figure 15: The relationship of the C_c with: (a) D_{50} and (b) C_u for different tailings.

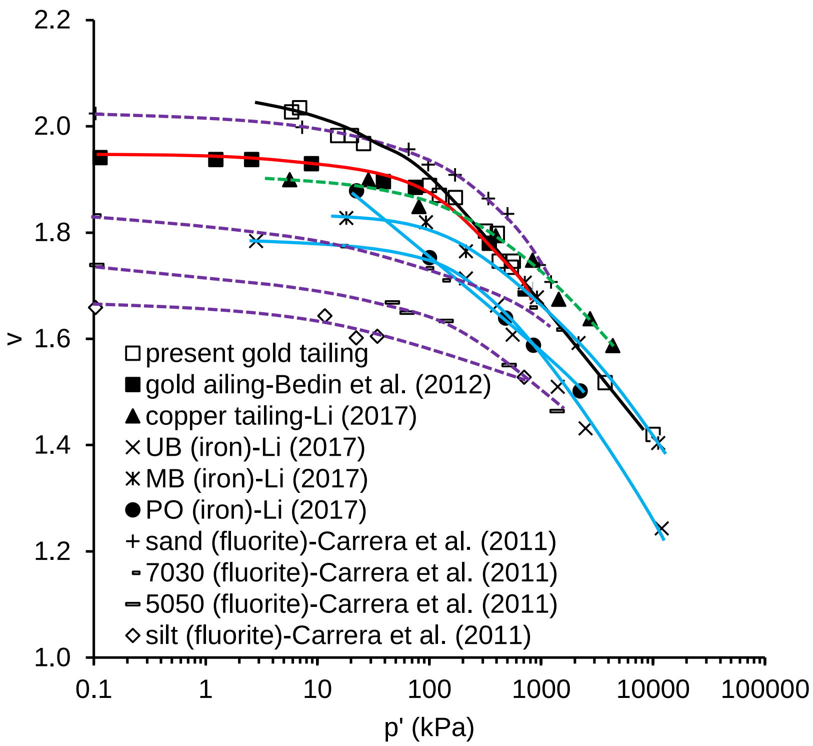

Figure 16: The CSLs of different tailings.

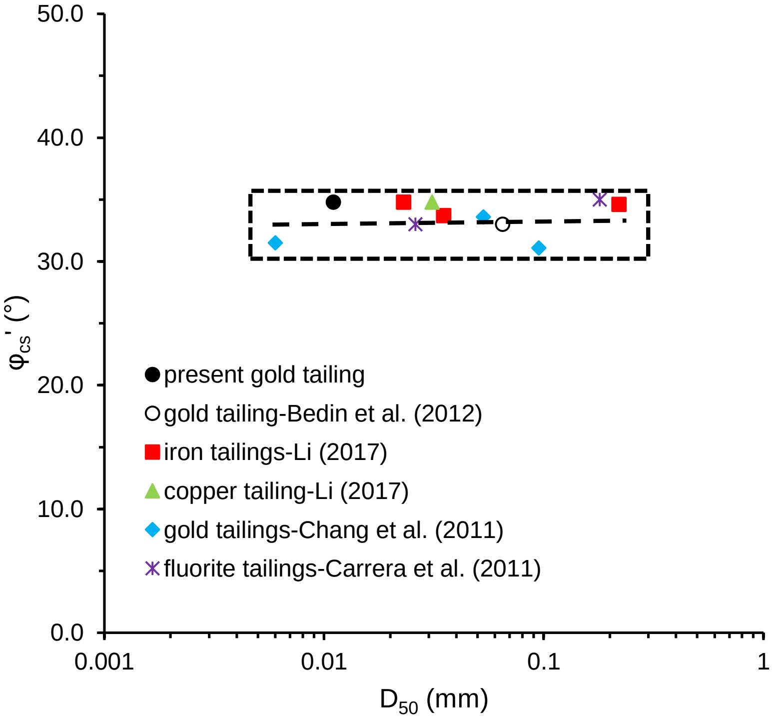

(a)

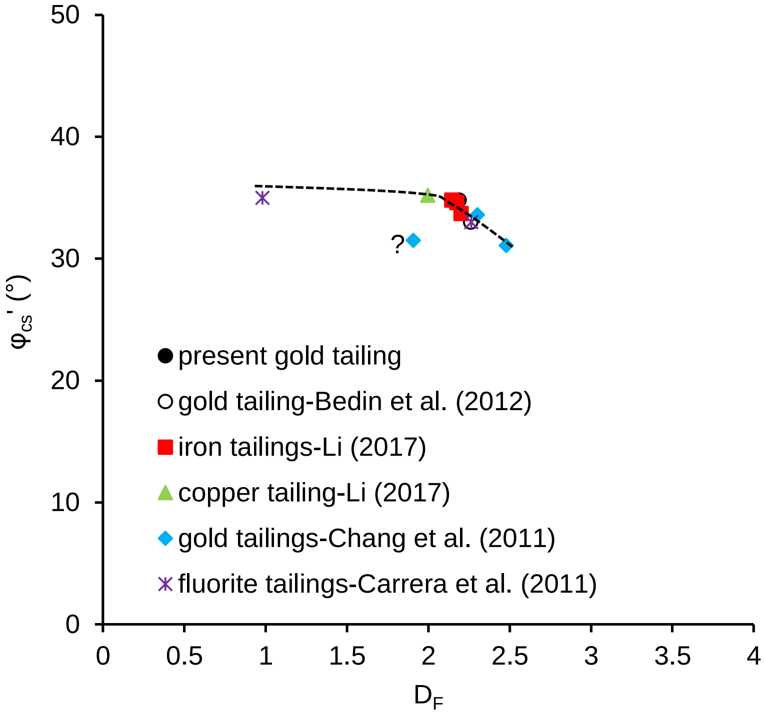

(b)

Figure 17: The relationship of the φ'_{cs} and the: (a) D_{50} and (b) D_F for different tailings.

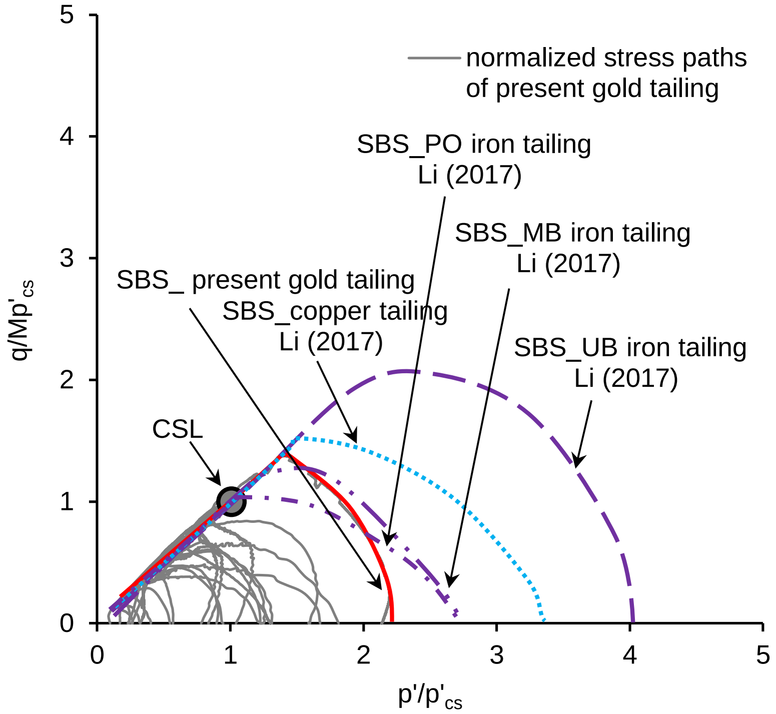

(a)

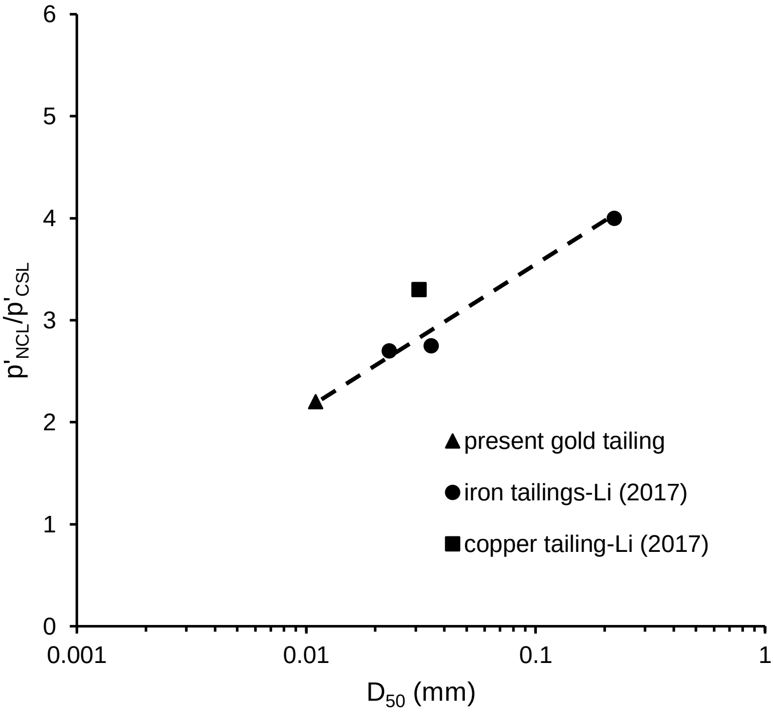

(b)

Figure 18: The (a) SBSs and (b) relationship of the stress ratio between isotropic NCL and CSL and the D_{50} for different tailings.

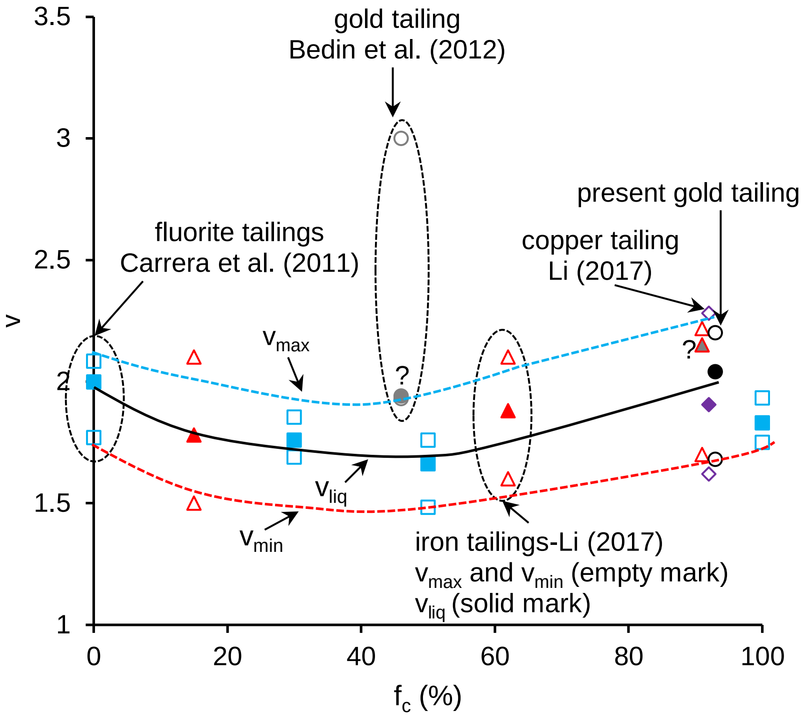

(a)

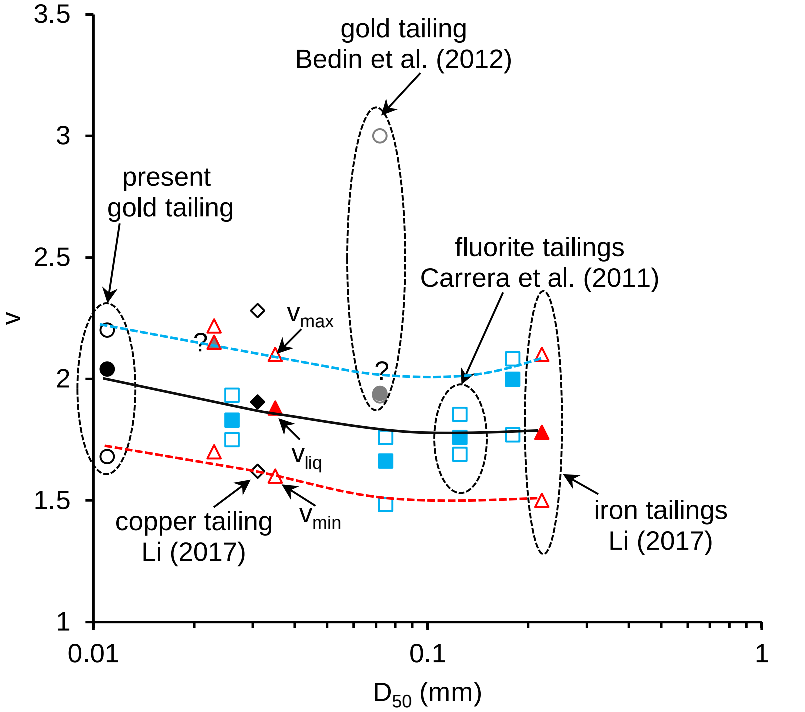

(b)

Figure 19: The relationships of the v_{liq}, v_{max} and v_{min} with: (a) f_c and (b) D_{50}.